Materials Science and Engineering A 529 (2011) 62–73

Contents lists available at SciVerse ScienceDirect

Materials Science and Engineering A

journal homepage: www.elsevier.com/locate/msea

General relationship between strength and hardness

P. Zhang, S.X. Li, Z.F. Zhang*

Shenyang National Laboratory for Materials Science, Institute of Metal Research, Chinese Academy of Sciences, Shenyang 110016, PR China

ARTICLE INFO

Article history:
Received 2 July 2011
Received in revised form 30 August 2011
Accepted 31 August 2011
Available online 8 September 2011

Keywords:
Crystalline materials
Bulk metallic glasses
Ceramics
Strength
Hardness
Yield criterion
Indentation

ABSTRACT

Both hardness and strength are the important properties of materials, and they often obey the three times empirical relationship in work-hardened metals and some bulk metallic glasses (BMGs). But the relationships between strength and hardness are quite different for those coarse-grained (CG) and ultrafine-grained materials, brittle BMGs and ceramics. In the present work, some Cu alloys with different microstructures, Zr-, Co-based BMGs and Al_2O_3 were employed to analyze the general relationship between hardness and strength. Several different relationships could be gotten from the experimental results of different materials available, and three types of indentation morphologies were observed. Indentation with "sink-in" morphology always represents a state of material and one third of hardness is in the range from yield strength to ultimate tensile strength. The other two indentation morphologies induced the fully hardening of material, so hardness could represent the intrinsic mechanical property of materials. The ratios of hardness to strength are found to be affected by the piled-up behaviors and their ability of shear deformation. Combined effect of the two aspects makes hardness approximately be three times of strength in the work-hardened crystalline materials and the shearable BMGs, but higher than three times of strength in the brittle-, annealed BMGs and ceramics.

1. Introduction

Hardness is one of the most characteristic properties of materials and often plays a key role in the progression of civilization because it has enabled progressively more sophisticated devices and machines to be constructed. However, the quantitative scales of hardness and related measurement methods were proposed only in recent one century or so. The first modern technique for measuring the hardness of metals is due to Brinell [1], who measured the hardness using a hard steel ball as the indenter. Then several other hardness tests have been developed, including the Vickers, Berkovich, Knoop and Rockwell tests [2–4]. The hardness value is usually defined as the ratio of the indentation load and either the surface or projected area of residual indents [3]. These standard hardness tests are vital in nearly all areas of materials science and engineering.

As an important property, hardness is of persistent interest to understand the relationships between hardness and other fundamental properties of materials and to address questions such as "*What is hardness? How does hardness depend on the mechanical properties and indenter geometry?*" [3,5]. On the other hand, a good understanding of the relationship between the hardness and tensile properties of materials is very important for several reasons [6]. First, reliable hardness–strength correlations allow for rapid overall mechanical property evaluations using fast and inexpensive hardness testing instead of elaborate tensile testing. Second, in contrast to tensile tests, the hardness of a material can be measured nondestructively in situ on fully assembled components and devices, thus allowing for structural integrity tests in service, for example, in elevated temperature applications. Third, several new materials could only be produced in small scale, these materials are insufficient to perform extensive tensile testing, hardness testing is often the only choice [7].

As early as 1945, Bishop et al. [8] suggested that the stress distribution under a conical indenter might be approximated by that of a spherical or cylindrical cavity. The relationships between the mean pressure under the indenter and Young's modulus and yield strength and work-hardening behaviors have been established. For elastic-perfect plastic solids, the pressure (P) at which the cavity extension depends on the ratio of Young's modulus (E) to yield strength (σ_y) and Poisson's ratio (ν) according to

$$\frac{P}{\sigma_y} = \frac{2}{3}\left(1 + \ln\frac{E}{3(1-\nu)\sigma_y}\right). \quad (1)$$

Following this idea, an extension of the spherical cavity was made by Johnson in the early 1970s [9]. He pointed out that the radial displacement of material lying on the elastic–plastic boundary must accommodate the volume of materials displaced by the indenter during indentation. Recently, Cheng and Cheng [5] also analyzed the relationship between hardness and strength based on the

* Corresponding author. Tel.: +86 24 23971043.
E-mail address: zhfzhang@imr.ac.cn (Z.F. Zhang).

0921-5093/$ – see front matter © 2011 Elsevier B.V. All rights reserved.
doi:10.1016/j.msea.2011.08.061

analysis of the dimension of indentation, they found that the ratio of hardness to yield strength was related to yield strength, Young's modulus, Poisson's ratio, work-hardening exponent and indenter half angle.

Besides these theoretical analyses, one empirical equation is widely used in lot of literatures [10–13], the relationship between the hardness H_V and yield strength σ_y approximately follows the form as below:

$$H_V \approx 3 \cdot \sigma_y. \quad (2)$$

Ashby and Jones [14] and Tabor [3] also established this 3-times relationship based on analyzing the five triangular portions of materials being tested and slip-line field of indentation, respectively. However, they also pointed out that this relationship is only valid for materials without work-hardening behavior, i.e. for ideally plastic materials [3,14]. For work-hardening metals, Tabor [3] suggested that the yield strength should be replaced by the uniaxial flow stress at some specified strain value. For a Vickers indenter, this representative strain is between 8% and 10%, and the hardness is then 3 times of the flow stress at this strain value. In other words, the work-hardening behavior could be induced by indentation, and one-third of the hardness value only represents the strength after hardening. Therefore, one question arises: *is hardness a property or a state of materials?*

On the other hand, both analyses by Ashby and Jones [14] and Tabor [3] relied on the relationship between the yield strength σ_y and critical shear fracture stress τ_0. They established this relationship based on the Tresca criterion and von Mises criterion [3]:

$$2\tau_0 = \frac{2}{\sqrt{3}}\sigma_y \approx 1.15\sigma_y \quad (\text{von Mises criterion}) \quad (3)$$

$$2\tau_0 = \sigma_y \quad (\text{Tresca criterion}). \quad (4)$$

In the Tresca criterion, the normal stress does not affect the shear stress on deformation plane. For the von Mises criterion, the effect of normal stress to shear deformation behavior is invariable in different materials. However, Zhang et al. [15,16] have proposed the promotion effect of the normal stress on the tensile shear fracture in bulk metallic glass (BMG). On the other hand, the finite element simulations of indentation were studied in the previous literatures [17,18], and the experimental observations well matched with the simulation results by considering the effect of normal stress on shear deformation. Therefore, the analyses by Ashby et al. and Tabor are not suitable for all the materials, such as crystalline materials, BMGs, and ceramics and so on.

Several publications reported the relationship between the ultimate tensile strength (UTS) and hardness [19,20]. An analysis of ASM handbook [19] exhibited the results of carbon and alloy steels with different pretreatments, and there is a fairly good relationship in the following form over a wide range of strengths,

$$H_V \approx 3 \cdot \sigma_{UTS} \quad (5)$$

Here, H_V is the Vickers hardness and σ_{UTS} is the UTS of materials. Therefore, another question is coming: *does one-third of hardness represent the yield strength or ultimate tensile strength in all the materials?*

To further improve the understanding of these problems above, in this study, we examine the hardness–strength data for three kinds of typical materials, including Cu and Cu–Zn alloys with different microstructures, various BMGs and ceramics. The influencing factors of the general relationship between strength and hardness are discussed in terms of the observed morphologies around the indentations.

2. Experimental procedure

To get the materials with different hardness and strength, several crystalline materials (commercially purity Cu, Cu–10 wt.%Zn, Cu–32 wt.%Zn), BMGs ($Zr_{52.5}Ni_{14.6}Al_{10}Cu_{17.9}Ti_5$ and $(Co_{0.942}Fe_{0.058})_{69}Nb_3B_{22.4}Si_{5.6}$) and ceramic ($Al_2O_3$) were selected. These Cu and Cu–Zn alloys were pretreated by several different methods. First, the polycrystalline Cu and Cu–Zn alloys were obtained by the cold-rolled/forged plates of Cu and Cu–Zn alloys annealed at 800 °C for 2 h. Second, the annealed Cu and Cu–Zn alloys were processed by equal channel angular pressing (ECAP) for 1–4 passes through a solid die having an angle of 90° between two channels [21]. After that the microstructures often consist of ultra-fine grains (100 nm–1 μm) and few nano-scale grains (below 100 nm). Third, to further refine the grains down to nano-scale, the annealed Cu–Zn alloys were processed by high-pressure torsion (HPT) for 1, 5, 10 turns, respectively [22].

Tensile specimens of the Cu and Cu–Zn alloys subjected to annealing, cold-rolling and ECAP were cut into a gauge length of 8 mm, with a width of 2 mm and a thickness of 1 mm. The Cu and Cu–Zn alloys subjected to HPT were cut into a gauge size of 2 mm × 1 mm × 1 mm. Tensile tests were carried out at room temperature (RT) with Instron 8871 or Instron E1000 testing machine operating at a strain rate of 5×10^{-4} s^{-1} for all the specimens.

The Vickers hardness was measured using an MH-5L Vickers micro-hardness tester. For these measurements, the specimen surfaces were carefully polished before testing. The tests were performed on the surfaces of samples using a typical diamond indenter in the form of pyramid with square base and an angle of 136° between opposite faces. A series of loads, from 0.98 N to 9.8 N, was applied for 15 s. The hardness of several alloys normally decreases with increasing the load, but finally the values of hardness for all specimens are invariable under high load. Finally, the stable value was chosen as the hardness of the specimens.

After analyzing the hardness and strength, several typical Cu and Cu–Zn alloys (Cu and Cu–32 wt.%Zn subjected to annealing, cold rolling, ECAP for 4 passes, and Cu–32 wt.%Zn subjected to HPT for 10 turns) were selected to investigate their deformation behaviors under hardness tests. The microstructures of these typical alloys with different pretreatments were observed by laser confocal microscope (LCM) LEXT OLS4000 and transmission electron microscopy (TEM) FEI Tecnai F20. Their morphologies of indentations, including all the Cu and Cu–Zn alloys, Zr-, and Co-based BMGs as well as Al_2O_3 ceramic were observed by LCM LEXT OLS4000.

3. Experimental results

3.1. Strength–hardness correlations in different materials

The strength and hardness of a series of Cu and Cu–Zn alloys are listed in Table 1. From these experimental data, one can find that the strength and hardness cover a relatively large range (63–969 MPa for yield strength, 223–1084 MPa for UTS and 523–2500 MPa for Vickers hardness). The ratio of hardness to strength is approximately equal to 3 in most Cu and Cu–Zn alloys, but obviously deviates from 3 in the annealed and HPT materials. To intuitively analyze the strength–hardness correlation in these materials, the Vickers hardness H_V has been plotted as functions of the strengths σ_y and σ_{UTS}, as shown in Fig. 1(a). Therefore, the relationship between hardness and strength could be classified into three types I, II, III, as shown in Fig. 1(a). One-third of hardness values of the annealed materials is always in the range from yield strength to UTS, thus, it is defined as the type I relationship:

$$\text{I}: \quad 3\sigma_y < H_V < 3\sigma_{UTS}. \quad (6)$$

Table 1
Strength, hardness and ratio of hardness to strength in Cu and Cu–Zn alloys with different pretreatment.

	σ (MPa)		H_V (MPa)	H_V/σ	
	σ_y	σ_{UTS}		H_V/σ_y	H_V/σ_{UTS}
Annealed Cu	80.71	223.43	545.86	6.76	2.44
Cold rolled Cu	250.03	271.28	925.81	3.70	3.41
Cu ECAP-1p	344.67	350.85	1194.18	3.46	3.40
Cu ECAP-2p	381.20	391.50	1253.34	3.29	3.20
Cu ECAP-3p	387.67	398.54	1263.19	3.26	3.17
Cu ECAP-4p	402.27	415.02	1329.86	3.31	3.20
Cu10%Zn ECAP-1p	375.87	389.97	1421.58	3.78	3.65
Cu10%Zn ECAP-2p	478.00	498.45	1565.72	3.28	3.14
Cu10%Zn ECAP-3p	531.70	546.43	1644.73	3.09	3.01
Cu10%Zn ECAP-4p	539.60	569.13	1691.32	3.13	2.97
Cu10%Zn HPT-1t	735.67	803.44	2046.80	2.78	2.55
Cu10%Zn HPT-5t	708.88	831.62	2105.72	2.97	2.53
Cu10%Zn HPT-10t	675.75	821.04	2130.74	3.15	2.60
Annealed Cu32%Zn	63.59	257.64	522.73	8.22	2.03
Cold rolled Cu32%Zn	374.35	422.86	1458.44	3.90	3.45
Cu32%Zn ECAP-1p	517.80	551.73	1847.54	3.57	3.35
Cu32%Zn ECAP-2p	648.90	685.27	2038.63	3.14	2.97
Cu32%Zn ECAP-3p	703.03	749.39	2038.31	2.90	2.72
Cu32%Zn ECAP-4p	734.63	768.27	2224.11	3.03	2.89
Cu32%Zn HPT-1t	918.31	1009.25	2415.99	2.63	2.39
Cu32%Zn HPT-5t	894.75	1035.44	2469.13	2.76	2.38
Cu32%Zn HPT-10t	968.76	1083.82	2500.69	2.58	2.31

With increasing the deformation degree during the pre-deformation, from cold-rolled to ECAP, the work-hardening ability of materials decreases gradually, and the yield strength σ_y is approximately equal to UTS σ_{UTS}. In these Cu and Cu–Zn alloys, the hardness approximates to three times of strength (yield strength or UTS), this is defined as the type II relationship:

$$\text{II}: \quad H_V \approx 3\sigma. \tag{7}$$

Here, σ represents the yield strength or UTS. Besides the two relationships above, a new type of correlation occurs in Cu–Zn alloys subjected to HPT. The one-third of hardness becomes lower than either yield strength or UTS:

$$\text{III}: \quad H_V < 3\sigma. \tag{8}$$

By the way, these experimental data of work-hardened materials do not significantly deviate from the three-time relationship, and the ratios of hardness to strength are in the range from 2.3 to 3.7.

On the other hand, the strength and hardness values of BMGs have been widely published in lots of literatures [17,23–33]. Here, several data about the strength and hardness of Zr-, Pd-, Fe-, Ti-, Cu-, Co-, Mg-based BMGs, which are collected from different publications [17,23–33], are listed in Table 2 and plotted in Fig. 1(b). Most of these experimental data obey the three-time relationship between hardness and strength, showing a good type II relationship. However, there are also several results deviated from the three-time relationship, as A, B, C, D shown in Fig. 1(b). The ratios of hardness to strength of BMGs A, B, C, D are equal to 3.84, 4.16, 6.30, 5.05, respectively. This correlation is classified as type IV relationship:

$$\text{IV}: \quad H_V > 3\sigma. \tag{9}$$

The main difference between the BMGs with different relationship is related to their plastic deformation abilities. The type III glasses always exhibit the shear deformation behaviors under either tension or compression [15,16], and the type IV glasses often display typical brittle fracture behavior even under compression [34,35]. The type IV glasses include the brittle BMGs and annealed BMGs. However, Co-based BMG, used in the present work, not only exhibited fragmental fracture behavior [36], but also obey three-time relationship.

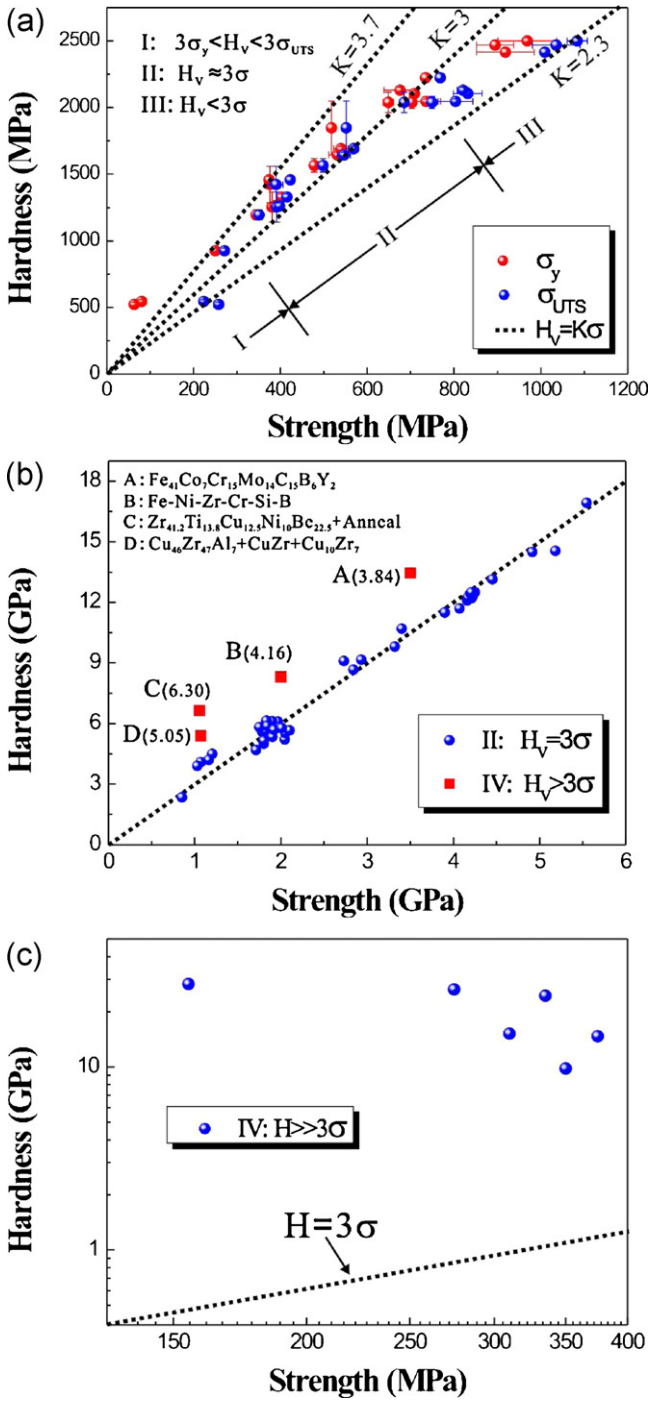

Fig. 1. The relationship between strength and hardness in: (a) Cu and Cu–Zn alloys with different pretreatment; (b) metallic glasses; (c) ceramics.

Besides, there are also several results about the strength and hardness of ceramics in the previous papers [37–40]. Here, several experimental data of different ceramics (PSZ, B_4C, Si_3N_4, Al_2O_3, SiC, TiB_2, MgO) as listed in Table 3 are plotted in Fig. 1(c). As brittle materials, ceramics always exhibit very high hardness in the range of 7.7–28.4 GPa (see Table 3) and relatively low strength of 97–375 MPa. Therefore, the ratio of hardness to strength obeys the type IV relationship, but the ratio value becomes extremely high, from 28 to 183 as the data listed in Table 3.

As mentioned above, the relationship between hardness and strength for all kinds of materials from ductile to brittle could be classified into 4 types, as shown in Eqs. (6)–(9). For better

Table 2
Strength, hardness and ratio of hardness to strength in metallic glasses.

	σ (GPa)	H_V (GPa)	H_V/σ	Investigators
$Zr_{52.5}Ni_{14.6}Al_{10}Cu_{17.9}Ti_5$	1.80	5.15	2.86	Present results
$(Co_{0.942}Fe_{0.058})_{69}Nb_3B_{22.4}Si_{5.6}$	3.32	9.82	2.96	
$Zr_{55}Cu_{30}Al_{10}Ni_5$	1.80	5.00	2.78	Keryvin [17]
$Pd_{40}Ni_{40}P_{20}$	1.78	5.60	3.15	
$Fe_{41}Co_7Cr_{15}Mo_{14}C_{15}B_6Y_2$	3.50	13.45	3.84	Keryvin et al. [32]
$Fe_{74}Ni_9Cr_4Si_3B_{10}$	2.93	9.16	3.13	Lee et al. [29]
$Fe_{66}Ni_7Zr_6Cr_8Si_3B_{10}$	2.00	8.31	4.16	
$Fe_{63}Ni_7Zr_6Cr_8W_3Si_3B_{10}$	2.73	9.10	3.33	
$Zr_{53}Cu_{30}Ni_9Al_8$	2.05	5.22	2.55	Jang et al. [31]
$(Zr_{53}Cu_{30}Ni_9Al_8)_{99.75}Si_{0.25}$	2.05	5.54	2.70	
$(Zr_{53}Cu_{30}Ni_9Al_8)_{99.5}Si_{0.5}$	1.82	5.64	3.10	
$(Zr_{53}Cu_{30}Ni_9Al_8)_{99.25}Si_{0.75}$	2.10	5.67	2.70	
$(Zr_{53}Cu_{30}Ni_9Al_8)_{99}Si$	1.75	5.82	3.33	
$Zr_{41.2}Ti_{13.8}Cu_{12.5}Ni_{10}Be_{22.5}$	1.95	5.95	3.06	Jun et al. [28]
Zr-400 °C × 5 min	1.97	6.10	3.10	
Zr-400 °C × 10 min	1.90	6.12	3.23	
Zr-400 °C × 20 min	1.83	6.14	3.36	
Zr-400 °C × 30 min	1.06	6.65	6.30	
$Zr_{41.2}Ti_{13.8}Cu_{12.5}Ni_{10}Be_{22.5}$	1.90	5.34	2.81	Raghavan et al. [27]
$Ti_{31.4}Zr_{36.6}Nb_7Cu_{5.9}Be_{19}$	1.20	4.50	3.74	Narayan et al. [33]
$Ti_{43}Zr_{25}Nb_7Cu_6Be_{19}$	1.16	4.20	3.61	
$Ti_{25}Zr_{43}Nb_7Cu_6Be_{19}$	1.07	4.10	3.83	
$Zr_{41}Ti_{14}Cu_{12.5}Be_{22.5}Ni_{10}$	1.84	5.88	3.20	Eckert et al. [23]
$Cu_{46}Zr_{47}Al_7$	1.99	5.80	2.91	Fan et al. [30]
$Cu_{46}Zr_{47}Al_7 + CuZr + Cu_{10}Zr$	1.92	5.70	2.97	
$Cu_{46}Zr_{47}Al_7 + CuZr + Cu_{10}Zr_7$	1.07	5.40	5.05	
$CuZr + Zr_2Cu$	1.03	3.90	3.79	
$[(Fe_{0.9}Co_{0.1})_{0.75}B_{0.2}Si_{0.05}]_{96}Nb_4$	3.90	11.50	2.95	Inoue et al. [26]
$[(Fe_{0.8}Co_{0.2})_{0.75}B_{0.2}Si_{0.05}]_{96}Nb_4$	4.17	12.25	2.94	
$[(Fe_{0.7}Co_{0.3})_{0.75}B_{0.2}Si_{0.05}]_{96}Nb_4$	4.20	12.45	2.96	
$[(Fe_{0.6}Co_{0.4})_{0.75}B_{0.2}Si_{0.05}]_{96}Nb_4$	4.25	12.50	2.94	
$[(Fe_{0.5}Co_{0.5})_{0.75}B_{0.2}Si_{0.05}]_{96}Nb_4$	4.21	12.20	2.90	
$[(Fe_{0.8}Co_{0.1}Ni_{0.1})_{0.75}B_{0.2}Si_{0.05}]_{96}Nb_4$	4.23	12.30	2.91	
$[(Fe_{0.6}Co_{0.1}Ni_{0.3})_{0.75}B_{0.2}Si_{0.05}]_{96}Nb_4$	4.07	11.70	2.87	
$[(Fe_{0.6}Co_{0.2}Ni_{0.2})_{0.75}B_{0.2}Si_{0.05}]_{96}Nb_4$	4.16	12.10	2.91	
$[(Fe_{0.6}Co_{0.3}Ni_{0.1})_{0.75}B_{0.2}Si_{0.05}]_{96}Nb_4$	4.20	12.40	2.95	
$Co_{43.5}Fe_{20}Ta_{5.5}B_{31.5}$	5.19	14.55	2.81	
$(Co_{0.535}Fe_{0.1}Ta_{0.055}B_{0.31})_{98}Mo_2$	5.55	16.93	3.05	
$[(Co_{0.535}Fe_{0.1}Ta_{0.055}B_{0.31})_{98}Mo_{0.02}]_{99}Si$	4.92	14.50	2.95	
$[(Co_{0.535}Fe_{0.1}Ta_{0.055}B_{0.31})_{98}Mo_{0.02}]_{98}Si_2$	4.45	13.14	2.95	
$(Fe_{0.75}B_{0.2}Si_{0.05})_{96}Nb_4$	3.40	10.70	3.15	Inoue *et al.* [24]
$[(Fe_{0.9}Co_{0.1})_{0.75}B_{0.2}Si_{0.05}]_{96}Nb_4$	3.90	11.50	2.95	
$[(Fe_{0.8}Co_{0.2})_{0.75}B_{0.2}Si_{0.05}]_{96}Nb_4$	4.17	12.25	2.94	
$[(Fe_{0.7}Co_{0.3})_{0.75}B_{0.2}Si_{0.05}]_{96}Nb_4$	4.20	12.45	2.96	
$[(Fe_{0.6}Co_{0.4})_{0.75}B_{0.2}Si_{0.05}]_{96}Nb_4$	4.25	12.50	2.94	
$[(Fe_{0.5}Co_{0.5})_{0.75}B_{0.2}Si_{0.05}]_{96}Nb_4$	4.21	12.50	2.97	
$Mg_{65}Cu_{7.5}Ni_{7.5}Zn_5Ag_5Y_{10}$	0.85	2.35	2.76	Pan et al. [25]
$Zr_{59}Cu_{20}Al_{10}Ni_8Ti_3$	1.71	4.69	2.74	
$Cu_{60}Zr_{30}Ti_{10}$	2.01	5.78	2.88	
$Fe_{65.5}Cr_4Mo_4Ga_4P_{12}C_5B_{5.5}$	2.84	8.67	3.05	

understanding of the relationship between strength and hardness, it is necessary to further reveal the microstructures, tensile stress–strain responses and indentation morphologies in detail. Therefore, several typical materials, including Cu and Cu–32 wt.%Zn after annealing, or processed by cold-rolling, ECAP for 4 passes and HPT for 10 turns, $Zr_{52.5}Ni_{14.6}Al_{10}Cu_{17.9}Ti_5$ (shear fracture under compression), $(Co_{0.942}Fe_{0.058})_{69}Nb_3B_{22.4}Si_{5.6}$ (fragmental fracture under compression) and Al_2O_3, were selected to be systematically investigated in following sections.

Table 3
Strength, hardness and ratio of hardness to strength in ceramics.

	σ (MPa)	H_V (GPa)	H_V/σ	Investigators
PSZ	350	9.8	28.00	Murray [38]
B_4C	155	28.4	183.23	
Si_3N_4	375	14.7	39.20	Shackelford [39]
Al_2O_3	310	15.2	49.03	Bauccio [37]
SiC	335	24.5	73.13	
TiB_2	275	26.5	96.36	
MgO	97	7.7	79.38	Schneider [40]

3.2. Microstructures and tensile properties of Cu and Cu–32 wt.%Zn alloys

The microstructures of annealed and cold-rolled Cu and Cu–32 wt.%Zn alloy were characterized using LCM, as shown in Fig. 2(a)–(d). The grain sizes could be measured to be 205 μm for the annealed Cu in Fig. 2(a), 300 μm for the annealed Cu–32 wt.%Zn alloy in Fig. 2(b), 25 μm for the cold-rolled Cu in Fig. 2(c), 100 μm for the cold-rolled Cu–32 wt.%Zn alloy in Fig. 2(d). In addition, TEM was used to characterize the microstructures of Cu and Cu–32 wt.%Zn alloy subjected to ECAP for 4 passes and Cu–32 wt.%Zn alloy subjected to HPT for 10 turns. The bright-field TEM micrographs of these three materials are shown in Fig. 2(e)–(h), and the small grains could be observed. The average grain sizes were measured in dark-field TEM micrographs to be 200 nm for Cu subjected to ECAP for 4 passes, 91 nm for Cu–32 wt.%Zn alloy subjected to ECAP for 4 passes and 34 nm in Cu–32 wt.%Zn alloy subjected to HPT for 10 turns.

The tensile engineering stress–strain curves of these Cu and Cu–Zn alloys are plotted in Fig. 3. In these curves, one can

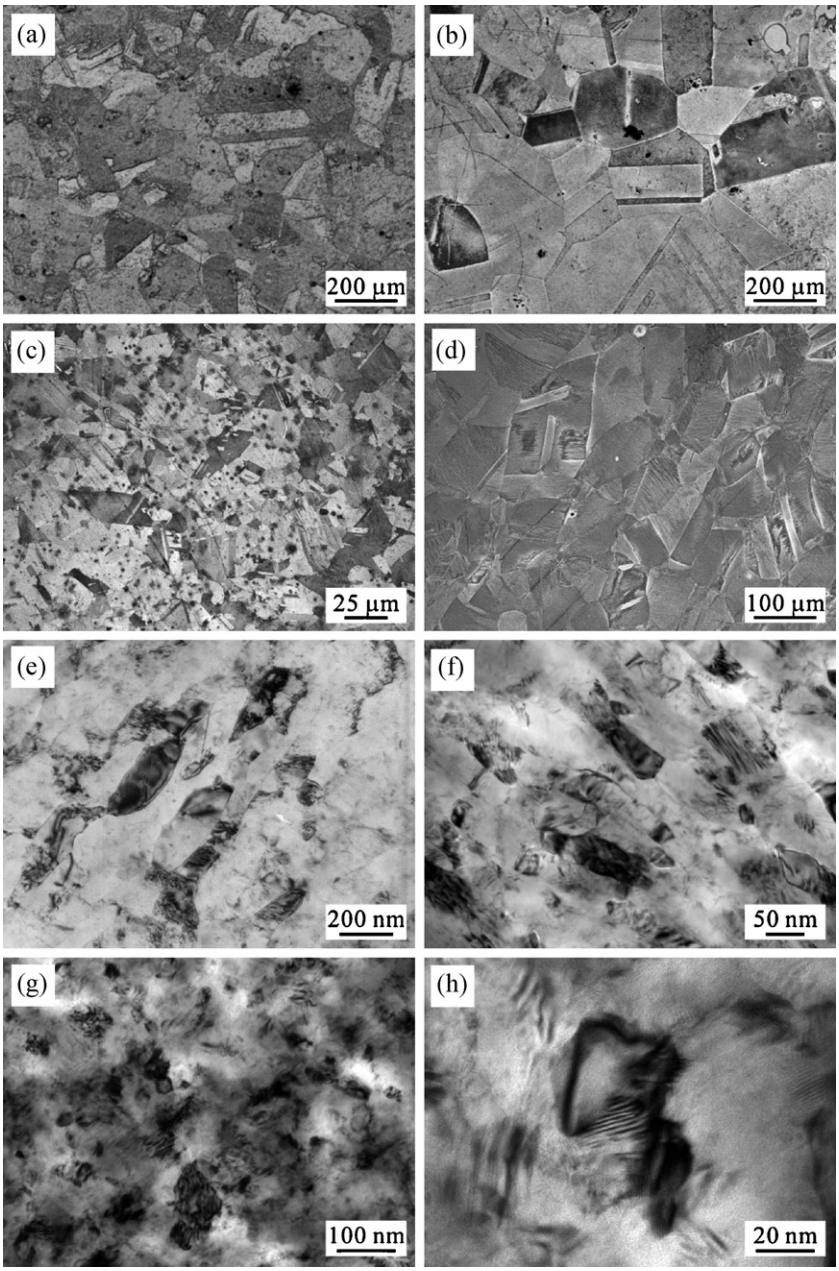

Fig. 2. Microstructures of Cu and Cu–Zn alloys observed by SEM: (a) annealed Cu; (b) annealed Cu–32 wt.%Zn; (c) cold-rolled Cu; (d) cold-rolled Cu–32 wt.%Zn; and by TEM: (e) Cu after ECAP for 4 passes; (f) Cu–32 wt.%Zn after ECAP for 4 pass; (g and h) Cu–32 wt.%Zn after HPT for 10 turns.

find that the strength increases with increasing the degree of pre-deformation, and the elongation decreases simultaneously. Annealed Cu and Cu–32 wt.%Zn alloy exhibit low strength, but relatively high work-hardening ability; annealed Cu could be hardened from 80 to 233 MPa and annealed Cu–32 wt.%Zn could be hardened from 64 to 258 MPa, respectively. After cold rolling, the work-hardening ability decreases in either Cu or Cu–32%Zn alloy, the difference between yield strength and UTS decreases to 8.4% and 13.1% of their yield strength in Cu and Cu–32 wt.%Zn alloy, respectively. In addition, it is interesting to find that the engineering stresses of cold-rolled Cu and Cu–32 wt.%Zn alloy approximately maintain constant in a large strain range after yielding. The work-hardening ability further decreases in Cu and Cu–32 wt.%Zn alloy subjected to ECAP for 4 passes, the differences between yield strength and UTS are 13 and 33 MPa (or 3.2% and 4.5% increment), respectively. Due to the difference in the specimen size of the HPT samples, the work-hardening behavior is not comparable to the other metals. However, the metals subjected to HPT for 10 turns suffered higher pre-deformation than the metals subjected to ECAP for 4 passes, so the work-hardening ability should be further decreased in the HPT samples.

In the previous studies, the correlation of hardness and strength was related to the work-hardening behavior of materials [3,5,8,9]. Therefore, these metals with different work-hardening abilities provide us an opportunity to study the influence of work-hardening ability on the ratio of hardness to strength.

3.3. Indentation morphologies of different materials

Geometry of indentations was classified into “sink-in” and “pile-up” morphologies in the previous studies, and the materials with different indentation morphologies always exhibit different relationship between hardness and strength [3]. To improve the understanding of this relationship, the morphologies

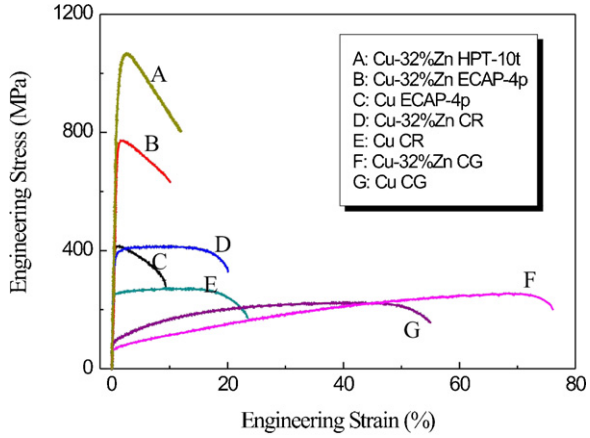

Fig. 3. Tensile engineering stress–strain curves of Cu and Cu–Zn alloys with different pretreatment.

of indentations were systematically observed using LCM in Cu and Cu–32 wt.%Zn alloys with different pretreatment, Zr-, Co-based BMGs and Al_2O_3, respectively.

3.3.1. Indentation morphologies of Cu and Cu–32 wt.%Zn

In annealed CG Cu and Cu–32 wt.%Zn alloy, the grain sizes are relatively large and the nucleation and movement of dislocations become much easy. When an indenter is penetrated into these specimens, the slip bands could nucleate easily and extend to a large area, as shown in Fig. 4(a). Since the shape of indentation is not a square, the edge should be not a straight line but bend to the center. From the 3-dimensional image in Fig. 4(b), the geometry of indentation could be observed directly, and the "sink-in" morphology is obvious. Comparing with the morphologies in Fig. 4(a) and (b), the curve edge in Fig. 4(a) could be thought as visual illusion caused by "sink-in". To analyze the deformation behavior of these CG materials, the sectional geometries across the center and two opposite edges of indentation (indicated as a straight line in Fig. 5(a) and (b) were measured using LCM. The experimental results of CG metals show that two sides of the indentation are relatively flat and the distribution of plastic deformation is relatively uniform in the area beside the indentation.

Meanwhile, the sectional geometries were also observed in Cu and Cu–32 wt.%Zn alloy subjected to cold-rolling, ECAP and HPT, as shown in Figs. 6 and 7. In these materials, the movement of dislocations is often restrained by other internal defects [41,42], and the plastic strain always concentrates near the indentation. Hence, the "pilling-up" morphologies could be obviously observed in all these materials, but the degrees of pilling-up are different. To compare the difference among these materials, the geometries of indentation were quantitatively measured, as shown by two parameters in the lower part of each picture in Figs. 6 and 7. The upper number means the range of pile-up and indentation ($2R$), and lower one means the range of indentation without pile-up ($2r$). The degree of pile-up (β) could be expressed by R and r as below:

$$\beta = \frac{R}{r}. \tag{10}$$

The experimental results show that β decreases from HPT Cu–32 wt.%Zn to CG materials. To understand the relationship between the geometry of indentation and the ratio of hardness to strength, the values of β are plotted versus the ratio of hardness to strength, as shown in Fig. 8. It can be seen that the ratio of hardness to strength decreases with decreasing the value β, and this ratio is equal to 3 when β approximates to 2.2, i.e. this ratio is affected by the pilling-up behavior near indentation.

3.3.2. Indentation morphologies of metallic glasses and ceramics

As mentioned above, the ratio of hardness to strength is also equal to 3 in those shearable BMGs and greater than 3 in the brittle BMGs and ceramic. Hence, the different geometries of indentations among these materials will be discussed in this section. The selected Zr- and Co-based BMGs respectively exhibit shear deformation and fragmental fracture behaviors under compression [36,43], and their sectional geometries were measured by LCM, as shown in Fig. 9. Both of two types of BMGs exhibit the "pilling-up" morphologies, and the values β, which were calculated from these figures, are about 1.99 and 1.89, respectively. Comparing with the results of Cu and Cu–32 wt.%Zn alloy, the three-times relationship between hardness and strength could be reached at a lower β. Therefore, the relationship between hardness and strength should be also affected by other factors except for the pilling-up behavior. Besides these observations, Keryvin et al. [32] have reported the sectional geometry of Fe-based BMG with higher ratio of hardness to strength (about 3.84). The value β of the Fe-based BMG is approximately equal to 1.89 and some local cracks can also be observed near the corner of indentation.

However, the ratio of hardness to strength is significantly increased to an extremely high value in ceramics, and the sectional geometry of indentation was measured in Al_2O_3, as shown in Fig. 10(a). It can be seen that the deformation around indentation is not a simple pilling-up behavior, some materials extrude in a large

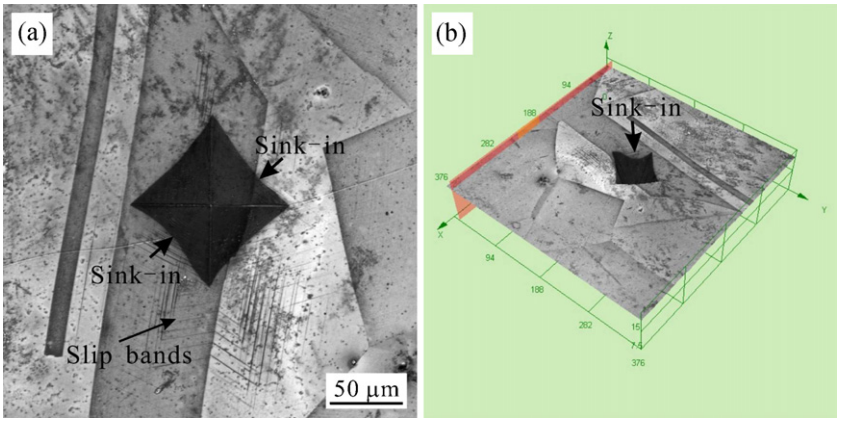

Fig. 4. (a) Two and (b) three dimensional sink-in morphology of annealed materials.

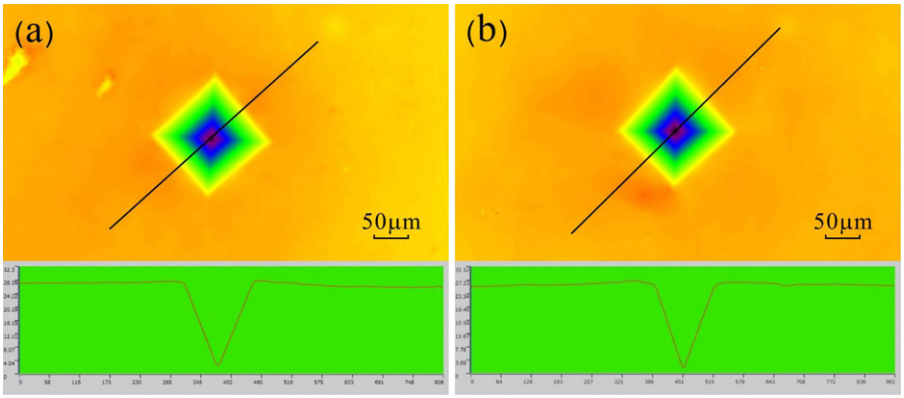

Fig. 5. Indentation morphologies in materials with type I relationship between strength and hardness: (a) annealed Cu; (b) annealed Cu–32 wt.%Zn.

range. Meanwhile, the cracking behavior could also be observed near the corner of indentation, as shown in Fig. 10(b). This cracking behavior is similar to the observation of Fe-based BMG [32], and could be attributed to the lack of shear deformation ability due to the brittleness.

4. Discussion

4.1. Classification of the indentation geometries

The geometry of indentations could be concluded into three types from the above observations shown in Figs. 4–7 and 9. Before discussing these different morphologies of indentations, the stress state under Vickers indenter should be firstly analyzed. When the square pyramid indenter penetrates into the specimen, materials near the edge are deformed by both normal stress and shear driven by the shear stress, but materials near the corner mainly deformed under the normal stress which could induce the corner cracking behaviors, as shown in Fig. 11. In materials with shear deformation ability, cracking behaviors near the corner are hardly to be observed, but the shear deformation near the edge is the main mechanism, the deformation behaviors could be discussed by using the idealized cavity model, as shown in Fig. 12. In this model, the deformed materials could be divided into three areas, as shown by A, B, C in Fig. 12. Due to the blocking of indenter, materials in area A could not extrude from the surface of specimen and are deformed under hydrostatic pressure. Meanwhile, the stress acted on materials in area C is lower than yield strength, so these materials are not plastically deformed. Therefore, the morphologies of indentations are decided by the deformation behaviors of materials in area B, and applied stress decreases with increasing the distance from indenter. On the other hand, the penetration of indenter is stopped

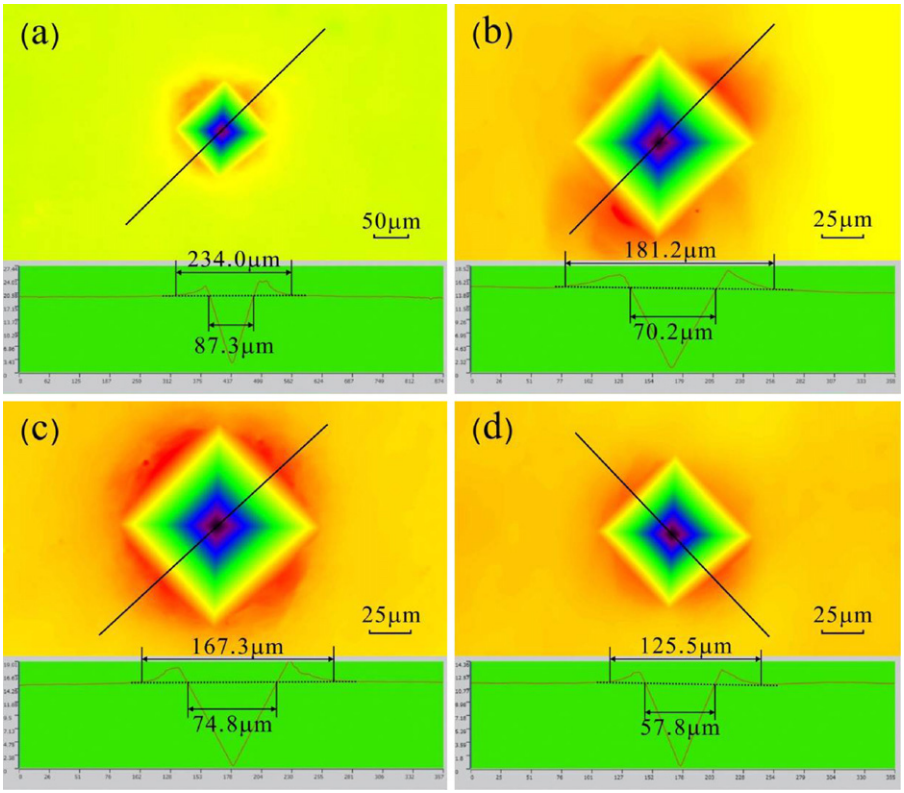

Fig. 6. Indentation morphologies in materials with type II relationship between strength and hardness: (a) cold rolled Cu; (b) cold rolled Cu–32 wt.%Zn; (c) Cu after ECAP for 4 passes; (d) Cu–32 wt.%Zn after ECAP for 4 passes.

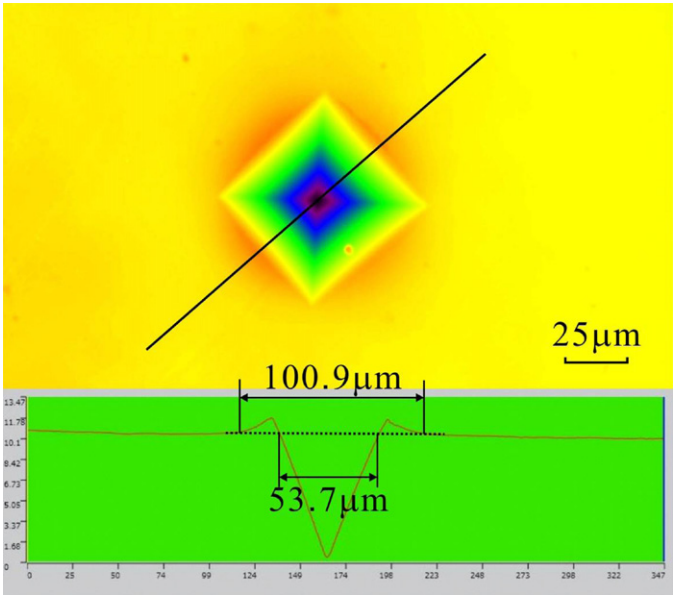

Fig. 7. Indentation morphology in material (Cu–32 wt.%Zn after HPT for 10 turns) with type III relationship between strength and hardness.

when balance between applied stress, F, and strength of hardened materials, $\sigma(\varepsilon_p)$:

$$H_V = \frac{F}{A} = C \cdot \sigma(\varepsilon_p), \tag{11}$$

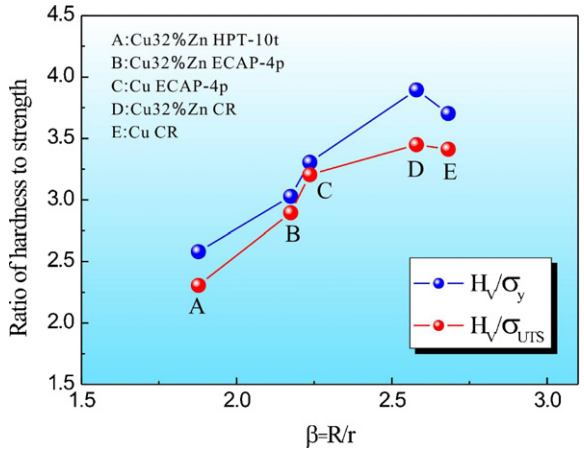

Fig. 8. Relationship between the ratio of hardness to strength and the piled-up behaviors of indentation in Cu and Cu–32 wt.%Zn with different pretreatments.

where, H_V is the Vickers hardness, A is the contact area and C is a constant.

Firstly, coarse-grained materials with good ductility always exhibit high work-hardening ability, such as annealed Cu and Cu–32 wt.%Zn. Materials near the indenter (see part A in Fig. 13(a)) are hardened by the applied plastic deformation, and the stress is not enough to induce further plastic deformation in this area. But the hardened part A could compress the materials around it (see part B in Fig. 13(a)), and make part B extrude to the free surface. Once the part B is hardened, it could also induce the plastic

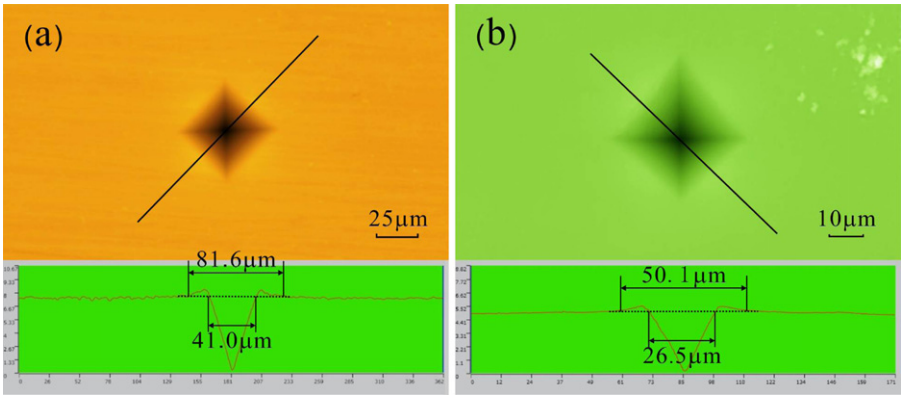

Fig. 9. Indentation morphology in materials of BMGs with type II and type IV relationship between strength and hardness: (a) Zr-based BMG; (b) brittle Co-based BMG.

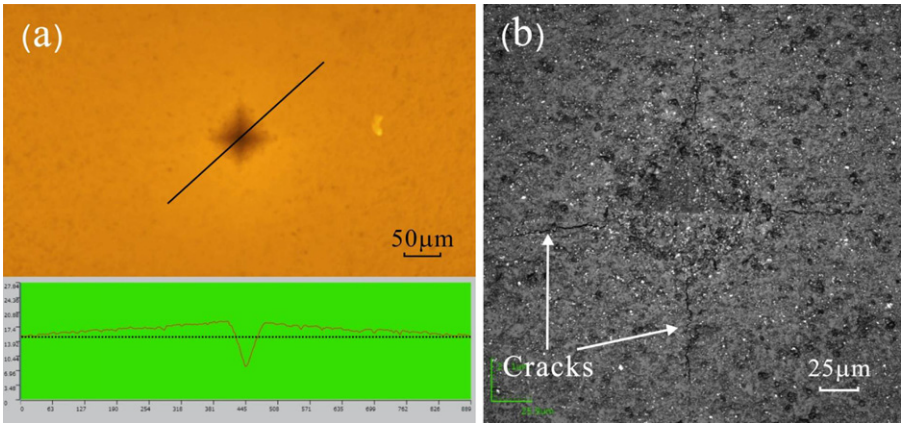

Fig. 10. Indentation morphology (a) and cracks (b) in Al_2O_3 with type IV relationship between strength and hardness.

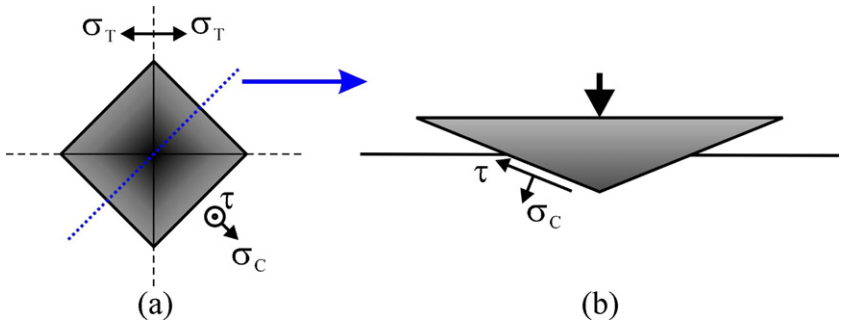

Fig. 11. Schematic illustration of the stress state near indentation.

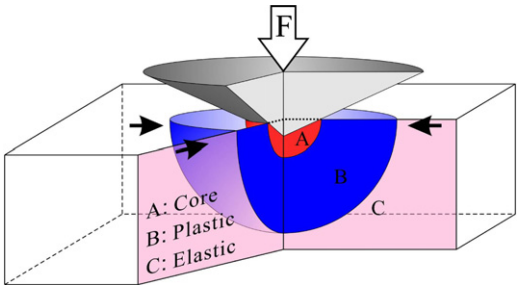

Fig. 12. Idealized cavity model of an elastic–plastic indentation.

deformation near it. Therefore, the plastic deformation could be uniformly extended in a relatively large range, which is related to the slip bands area in the surface, as shown in Fig. 13(d). Therefore, the balance in Eq. (11) could be reached by increasing contact area, and the strength of hardened materials is retained in a suitable value. Following the suggestion of Tabor, one third of hardness represents the strength after a special tensile elongation, about 8–10% [3]. Therefore, this type of materials cannot be fully hardened to their UTS, and the measured hardness only represents the stress level under certain strain, but not the intrinsic property of these materials.

After pre-deformation from CG materials, the plastic deformation induced by hardness test always concentrates near indentation. It could be schematically illustrated in Fig. 13(b) and (e), the materials near indentation are continuously hardened but cannot induce the plastic deformation far away from the indentation. Therefore, the plastic deformation was only concentrated in a relatively small area near the indentation, which will lead to the second type of "pile-up" morphology. In this type of materials, the ductility is decreased to a relatively low level due to the limitation of the nucleation and movement of dislocations. The piled-up materials near the indentation could be hardened to UTS much easier due to the lack of ductility and concentration of plastic deformation. In other words, the hardness of these materials could represent the intrinsic property related to UTS. Besides, one third of hardness is approximately equal to UTS, but the ratio of hardness to UTS slightly deviates from 3 in the materials with different degrees of pilling-up. The typical materials in this study include the Cu and Cu–Zn alloys after cold-rolling, ECAP and HPT processing, as well as Zr-based BMGs.

With further decreasing the plastic deformation ability, the materials become much brittle and the extrusion behaviors under the penetration of indenter are greatly limited. In this case, the normal stress (indicated as σ in Fig. 13(f)) near the corner becomes more important, which will induce the local cracking around the indentation. Since the restriction of materials near the edge of indentation will be relaxed after the local cracking, the shear deformation could extend to far away from indentation. This morphology is being sorted as the third type of "crack" morphology. This type of materials have no work hardening ability under tensile stress, the hardness is related to the fracture strength of materials. However, the limitation of around materials could induce high fracture strength of materials. Therefore, one third of hardness of these materials is higher than the fracture strength, and hardness could not represent the intrinsic property.

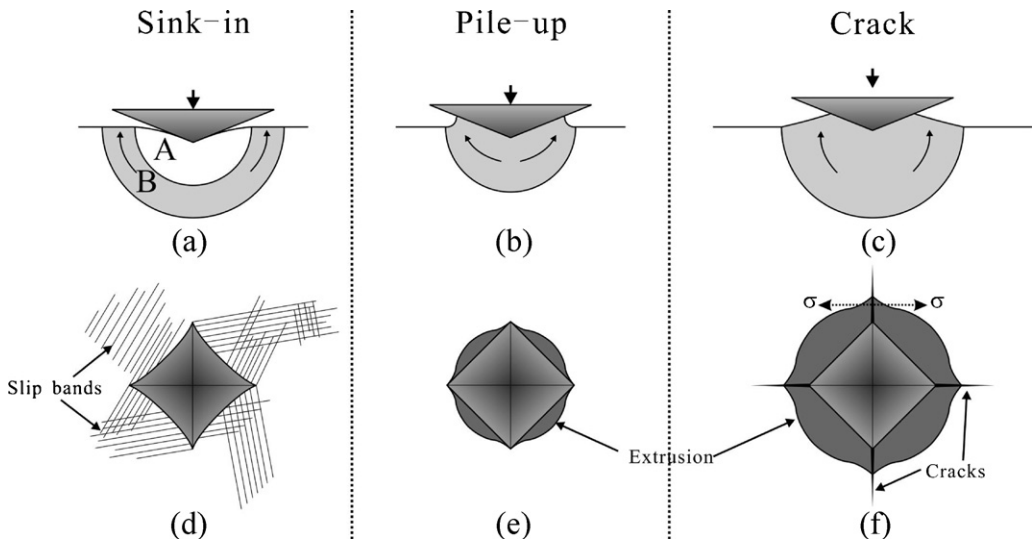

Fig. 13. Schematic illustration of three types of indentation morphologies.

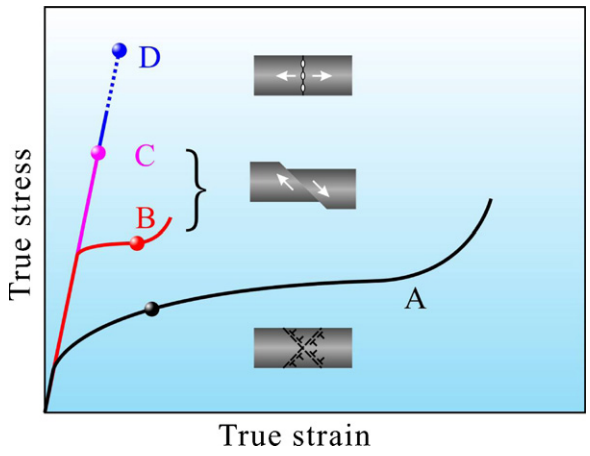

Fig. 14. Schematic illustration of true stress–strain curves of different materials.

Considering the tensile behaviors, the three types of materials could be illustrated as Fig. 14. Material A represents materials with good ductility (such as annealed Cu and Cu–Zn alloys), which always exhibit "sink-in" morphology after hardness test, and the hardness is a work hardened state of materials. Material D represents brittle materials with low ductility and toughness (such as BMGs with normal fracture feature under tensile tests), one third of hardness is always higher than tensile fracture strength. Materials B and C always exhibit shear deformation behaviors under tensile test, and the hardness is one intrinsic property of material. Therefore the relationship between hardness and strength in materials B and C will be detailed discussed, and then other types materials will be compared with it.

4.2. General relation between strength and hardness

Since the materials with relatively high ductility could not be fully hardened under hardness test, their indentations always exhibit "sink-in" morphologies. Therefore, one third of hardness is lower than its UTS due to the insufficient hardening. However, the hardness in the materials with "pile-up" morphologies could be fully hardened when indenter penetrates. The deformed materials under indenter are restricted by materials around them, and the extrusion imposed by shearing becomes the major deformation mode. Thus the slip-line field theory was introduced to study the correlation between Vickers hardness (H_V) and shear strength (τ_0) by Tabor [3], as schematically illustrated in the left part of Fig. 15. Following his analysis, this correlation is affected by "pile-up" morphology, which could be represented by rotated angle (θ) between the slip-line of free and contact surfaces [3]:

$$\frac{H_V}{\tau_0} = 2\ \sin 68^\circ \cdot (1+\theta) \approx 1.8544\,(1+\theta). \tag{12}$$

This analysis neglects the friction between indenter and contact material, so the ratio of hardness to shear strength always deviates from 1.8544 $(1+\theta)$. However, it can be concluded that this ratio would be affected by changing θ. Both θ and β could represent the "pile-up" morphology, so the variation of θ always companies with the change of β. To analyze the relationship between θ and β, the volume of materials is proposed to be invariable during penetration by indenter, i.e. $A_1 = A_2$ in the right part of Fig. 15. After analyzing the geometries of A_1 and A_2, this relationship could be expressed as:

$$\beta = \frac{R}{r} = \frac{h_1+h_2}{h_2} = 1 + \sqrt{1 + \frac{\tan\left(\frac{\pi}{2}+\theta-\alpha\right)}{\tan\alpha}}. \tag{13}$$

where, h_1, h_2, R, r and α are indicated in Fig. 15, respectively. Considering Eqs. (3), (4), (12) and (13) together, a higher β could induce a higher ratio of hardness to strength, which is consistent with the experimental results shown in Fig. 8. Here, σ_y used in Eqs. (3) or (4) represents the yield strength of hardened materials, which is approximately equal to the UTS of the materials without plastic deformation.

In addition to the analysis above, the relationship between σ_y and τ_0 can also be established based on the Tresca criterion or von Mises criterion. However, these criteria are not suitable for the analysis on the BMGs and ceramics due to the normal stress effect on the shear strength [15–18]. Zhang and Eckert [44] have proposed a unified tensile fracture criterion to describe all the possible failure modes of various materials by defining a new parameter, i.e. the ratio $\alpha = \tau_0/\sigma_0$. The ratio of $2\tau_0$ to σ_y (M) is affected by the interaction between normal and shear strength, i.e. the ratio $\alpha = \tau_0/\sigma_0$. Here, σ_y also represents the yield strength of hardened materials, which is approximately equal to the UTS of materials without plastic deformation. Therefore, M could be expressed as:

$$M = \frac{2\tau_0}{\sigma_{UTS}} = \begin{cases} \dfrac{1}{\sqrt{1-\alpha^2}}, & \alpha < \sqrt{2}/2 \\ 2\cdot\alpha, & \alpha \geq \sqrt{2}/2 \end{cases} \tag{14}$$

where, σ_{UTS} means the UTS of materials. Considering Eqs. (11)–(13) together, the ratio of hardness to strength could be expressed as:

$$\frac{H_V}{\sigma_{UTS}} = \Phi(M, \beta). \tag{15}$$

Increasing either M or β could induce the increase of H_V/σ_{UTS}.

Besides the effect of M, α is also related to the shear deformation ability of materials, and could affect the "pile-up" morphology of indentations. When α is relatively low, the shear ability is not enough to make the plastic deformation concentrate in a small area, leading to a "sink-in" morphology around the indentation.

The "pilling-up" morphology is mainly affected by ability of work-hardening, and this effect in spherical indentation has been proposed as [45]:

$$\left(\frac{h_1+h_2}{h_1}\right)^2 = \frac{a^2}{a*^2} = \frac{5}{2}\cdot\frac{(2-n)}{(4+n)}, \tag{16}$$

where, h_1, h_2, a^* and a are indicated in Fig. 16, and n means the hardening rate of materials. Considering Eqs. (13) and (16) together, reducing β value could be induced by decreasing the hardening rate. On the other hand, the shear ability continuously decreases when the work-hardening ability decreases from the materials after CR to ECAP and then to HPT, i.e. α increases with decreasing n. Thus, the reduction of β value could be induced by increasing α when α is small. However, the work-hardening ability decreases to very low level (zero under tension) in shearable, and brittle BMGs as well as ceramics. In these materials, β is mainly affected by the shear ability. Lower shear ability (increasing α) imposed that the materials with the same volume could only accommodate few plastic deformation, i.e. the same plastic deformation should extend to a larger area (increasing β). By the way, the loss of shear ability either makes the cracking nucleation easy because the cracking

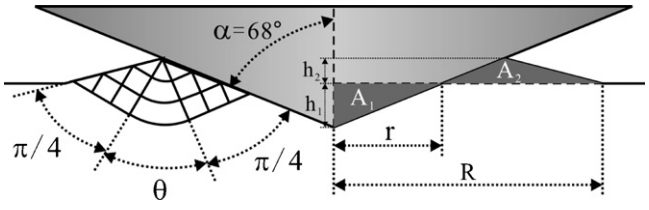

Fig. 15. Schematic illustration of piled-up behavior near pyramid indentation.

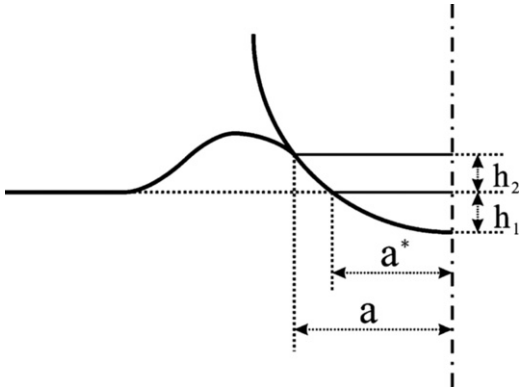

Fig. 16. Schematic illustration of piled-up behavior near spherical indentation.

could relax the restriction of materials, or makes the plastic deformation extend to a large much easy. Therefore, the "pilling-up" parameter β firstly decreases and then increases with increasing α, as schematically illustrated by the blue line in Fig. 17.

Following the above analysis and Eq. (14), both M and β are plotted versus α in Fig. 17. It can be seen that M only slightly increases, but β decreases more obviously with increasing α for crystalline materials. Therefore, the ratio of hardness to strength slightly decreases with decreasing β, but does not obviously deviate from 3. With further increasing α, the decrease of β becomes more slow, and the increase of M becomes little higher in those shearable BMGs than in crystalline materials. The combined effects of M and β make the shearable BMGs approximate to the three-time relationship, and three-time relationship induced by higher M could be achieved with lowering β in BMGs than crystalline materials. However, the variation of M becomes much quickly when α is greater than 0.707, i.e. in the brittle BMGs, annealed BMGs and ceramics. The cracks always nucleate under indenter in these materials, which makes β also increase significantly. Hence, the ratio of hardness to strength increases quickly to an extremely high level gradually. Particularly, Co-based BMG is brittle but near to the regime of the shearable BMGs, and also obeys the three-time relationship.

Following the above analyses, the ratio of hardness to strength should be related to the difference in the shear ability of various materials, which is schematically plotted versus α in Fig. 18. The materials with high ductility could be easily deformed by the easy nucleation and movement of dislocations because they could not be fully hardened during the hardness test. Hence, one third of hardness is always lower than its UTS. For the micron-grained (MG), ultra-fine grained (UFG), nanocrystalline (NC) materials and

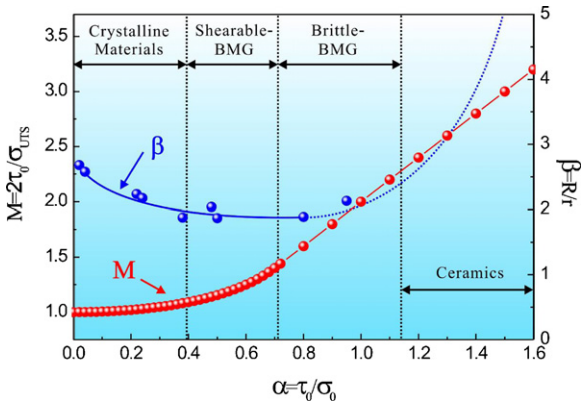

Fig. 17. Plots of M and β versus α in crystalline materials, BMGs and ceramics.

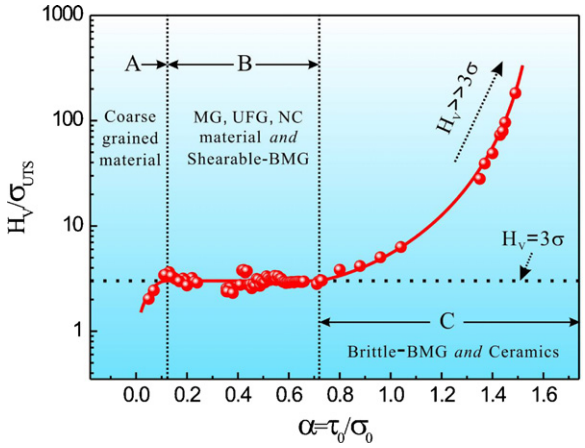

Fig. 18. Schematic illustration of the ratio of hardness to UTS with increasing the value α in crystalline materials, BMGs and ceramics.

shearable BMGs, the trend for shear deformation should be gradually increased (e.g. increasing the value α), they should be easily hardened up to their UTS. Therefore, the hardness and strength will approximately follow the three-time relationship. However, the ratio of hardness to strength becomes greater than 3 for those brittle BMGs and ceramics, because the fracture strength increases under indentation due to the limitation of around materials, and the shear deformation tends to be extremely difficult and the cleavage cracking becomes much easy. Therefore, it could be concluded that the three-time relationship could only be used in those materials with low work-hardening ability and difficult to normal cracking.

5. Conclusions

Based on the experimental results of CG to nanocrystalline Cu and Cu–Zn alloys, Zr-, Co-based BMGs and Al_2O_3, the relationship between hardness and strength is systematically discussed and analyzed, and the following conclusions can be drawn:

(a) The geometry of indentations could be classified into three types: "sink-in", "pile-up" and "crack". The hardness of materials with "sink-in" morphology only represents a hardened state of material. The hardness of materials with "crack" morphology is related to the fracture behavior, but different with the tensile fracture strength due to different stress state. However, the hardness of materials with "pile-up" morphology could represent the intrinsic property of materials.

(b) The relationships of hardness and strength in materials with "pile-up" morphology are affected by interactions between normal and shear stresses and the pilling-up behaviors of materials during penetration of indenter. The combined effect of the two aspects makes the hardness and strength obey the three-time relationship in crystalline materials and the shearable BMGs.

(c) The ratio of hardness to UTS is lower than 3 in the materials with good ductility (such as annealed Cu and Cu–Zn alloys), due to the hardness represents a hardened state of materials without fully hardened. But this ratio is increased to a high level in materials, which exhibit normal fracture behavior in tensile test, this could be attributed to the different fracture strength under hardness and tensile test, by the way, the lower shear-ability and the cleavage cracking becomes much easy also could induce the increase in the ratio. The three-time relationship can be well maintained only in those materials with mediate shear ability and normal fracture becomes very difficult.

Acknowledgements

The authors would like to thank W. Gao, X.H. An, Q.Q. Duan, M.J. Zhang and R.B. Figueiredo for sample preparation, mechanical tests, SEM and TEM observations. This work was financially supported by the National Natural Science Foundation of China (NSFC) under grant Nos. 50625103, 50890173 and 50931005, and the National Basic Research Program of China under grant No. 2010CB631006.

References

[1] J.A. Brinell, Mémoire sur les épreaves á bille en acier, II. Cong. Int. Methodes d'Essai, A. Wahlberg, Paris, 1900. For the first english account see, 1901, p. 243.
[2] B.W. Mott, Micro-indentation Hardness Testing, Butterworths, London, 1956.
[3] D. Tabor, Hardness of Metals, Clarendon Press, Oxford, 1951.
[4] M. Bauccio (Ed.), ASM Metals Reference Book, ASM International, Materials Park, OH, 1993.
[5] Y.-T. Cheng, C.-M. Cheng, Mater. Sci. Eng. R 44 (2004) 91–149.
[6] I. Brooks, P. Lin, G. Palumbo, G.D. Hibbard, U. Erb, Mater. Sci. Eng. A 491 (2008) 412–419.
[7] Y.P. Li, X.F. Zhu, G.P. Zhang, J. Tan, W. Wang, B. Wu, Philos. Mag. 90 (2010) 3049–3067.
[8] R.F. Bishop, R. Hill, N.F. Mott, Proc. Phys. Soc. 57 (1945) 147–159.
[9] K.L. Johnson, J. Mech. Phys. Solids 18 (1970) 115–126.
[10] X.H. An, S.D. Wu, Z.F. Zhang, R.B. Figueiredo, N. Gao, T.G. Langdon, Scr. Mater. 63 (2010) 560–563.
[11] H. Li, F. Ebrahimi, Mater. Sci. Eng. A 347 (2003) 93–101.
[12] L. Lu, R. Schwaiger, Z.W. Shan, M. Dao, K. Lu, S. Suresh, Acta Mater. 53 (2005) 2169–2179.
[13] P.G. Sanders, C.J. Youngdahl, J.R. Weertman, Mater. Sci. Eng. A 234–236 (1997) 77–82.
[14] M.F. Ashby, D.R.H. Jones, Engineering Materials, Pergamon, Oxford, 1980.
[15] Z.F. Zhang, J. Eckert, L. Schultz, Acta Mater. 51 (2003) 1167–1179.
[16] Z.F. Zhang, G. He, J. Eckert, L. Schultz, Phys. Rev. Lett. 91 (2003) 045505.
[17] V. Keryvin, Acta Mater. 55 (2007) 2565–2578.
[18] R. Vaidyanathan, M. Dao, G. Ravichandran, S. Suresh, Acta Mater. 49 (2001) 3781–3789.
[19] H.E. Boyer, T.L. Gall (Eds.), Metals Handbook, Desk Edition, ASM International, Metals Park, Ohio, 1985.
[20] W.D. Callister Jr., Materials Science and Engineering – An Introduction, John-Wiley, NewYork, 1992.
[21] S. Qu, X.H. An, H.J. Yang, C.X. Huang, G. Yang, Q.S. Zang, Z.G. Wang, S.D. Wu, Z.F. Zhang, Acta Mater. 57 (2009) 1586–1601.
[22] M. Kawasaki, T.G. Langdon, Mater. Sci. Eng. A 498 (2008) 341–348.
[23] J. Eckert, A. Kubler, L. Schultz, J. Appl. Phys. 85 (1999) 7112–7119.
[24] A. Inoue, B.L. Shen, C.T. Chang, Acta Mater. 52 (2004) 4093–4099.
[25] X.F. Pan, H. Zhang, Z.F. Zhang, M. Stoica, G. He, J. Eckert, J. Mater. Res. 20 (2005) 2632–2638.
[26] A. Inoue, B.L. Shen, C.T. Chang, Intermetallics 14 (2006) 936–944.
[27] R. Raghavan, P. Murali, U. Ramamurty, Intermetallics 14 (2006) 1051–1054.
[28] H.-J. Jun, K.S. Lee, Y.W. Chang, Mater. Sci. Eng. A 449–451 (2007) 526–530.
[29] K.A. Lee, Y.C. Kim, J.H. Kim, C.S. Lee, J. Namkung, M.C. Kim, Mater. Sci. Eng. A 449–451 (2007) 181–184.
[30] J.T. Fan, Z.F. Zhang, F. Jiang, J. Sun, S.X. Mao, Mater. Sci. Eng. 487 (2008) 144–151.
[31] J.S.C. Jang, S.R. Jian, C.F. Chang, L.J. Chang, Y.C. Huang, T.H. Li, J.C. Huang, C.T. Liu, J. Alloys Compd. 478 (2009) 215–219.
[32] V. Keryvin, V.H. Hoang, J. Shen, Intermetallics 17 (2009) 211–217.
[33] R.L. Narayan, K. Boopathy, I. Sen, D.C. Hofmann, U. Ramamurty, Scr. Mater. 63 (2010) 768–771.
[34] Z.F. Zhang, F.F. Wu, W. Gao, J. Tan, Z.G. Wang, M. Stoica, J. Das, J. Eckert, B.L. Shen, A. Inoue, Appl. Phys. Lett. 89 (2006) 251917.
[35] Z.F. Zhang, H. Zhang, B.L. Shen, A. Inoue, J. Eckert, Philos. Mag. Lett. 86 (2006) 643–650.
[36] J.W. Cui, Unpublished data.
[37] M. Bauccio (Ed.), ASM Engineering Materials Reference Book, ASM International, Materials Park, OH, 1994.
[38] G.T. Murray, Handbook of Materials Selection for Engineering Applications, CRC Press, California Polytechnic State University, San Luis Obispo, CA, 1997.
[39] J.F. Shackelford (Ed.), CRC Materials Science and Engineering Handbook, CRC Press, Boca Raton, 1994.
[40] S.J.J. Schneider (Ed.), Engineered Materials Handbook, ASM International, Metals Park, OH, 1991.
[41] T.G. Langdon, R.Z. Valiev, Prog. Mater. Sci. 51 (2006) 881–981.
[42] R.Z. Valiev, R.K. Islamgaliev, I.V. Alexandrov, Prog. Mater. Sci. 45 (2000) 103–189.
[43] J.X. Zhao, F.F. Wu, R.T. Qu, S.X. Li, Z.F. Zhang, Acta Mater. 58 (2010) 5420–5432.
[44] Z.F. Zhang, J. Eckert, Phys. Rev. Lett. 94 (2005) 094301.
[45] R. Hill, B. Storakers, A.B. Zdunek, Proc. R. Soc. Lond. 423 (1989) 301–330.